PNAS RESEARCH ARTICLE | CELL BIOLOGY

A targeted combination therapy achieves effective pancreatic cancer regression and prevents tumor resistance

Vasiliki Liaki[a,1], Sara Barrambana[a,1], Myrto Kostopoulou[a], Carmen G. Lechuga[a], Elena Zamorano-Dominguez[a,b], Domingo Acosta[a], Lucia Morales-Cacho[a], Ruth Álvarez[a], Pian Sun[a], Blanca Rosas-Perez[a], Rebeca Barrero[a], Silvia Jiménez-Parrado[a], Alejandra López-García[a], Marta San Roman[a], Juan Carlos López-Gil[a], Matthias Drosten[b,c], Bruno Sainz Jr.[b,d,e], Monica Musteanu[b,f,g], Eduardo Caleiras[h], Nelson Dusetti[i], Valeria Poli[i], Francisco Sánchez-Bueno[k], Carmen Guerra[a,b,2,3], and Mariano Barbacid[a,b,2,3]

Affiliations are included on p. 10.

Contributed by Mariano Barbacid; received August 25, 2025; accepted November 3, 2025; reviewed by Anton Berns, Ignacio Garrido-Laguna, and David A. Tuveson

Pancreatic ductal adenocarcinoma (PDAC) has one of the lowest cancer survival rates. Recent studies using RAS inhibitors have opened the door to more efficacious therapies, although their beneficial effect is still limited mainly due to the rapid appearance of tumor resistance. Here, we demonstrate that genetic ablation of three independent nodes involved in downstream (RAF1), upstream (EGFR), and orthogonal (STAT3) KRAS signaling pathways leads to complete and permanent regression of orthotopic PDACs induced by KRAS/TP53 mutations. Likewise, a combination of selective inhibitors of KRAS (RMC-6236/daraxonrasib), EGFR family (afatinib), and STAT3 (SD36) induced the complete regression of orthotopic PDAC tumors with no evidence of tumor resistance for over 200 d posttreatment. This combination therapy also led to significant regression of genetically engineered mouse tumors as well as patient-derived tumor xenografts (PDX) in the absence of tumor relapses. Of importance, this combination therapy was well tolerated. In sum, these results should guide the development of new clinical trials that may benefit PDAC patients.

Pancreatic Ductal Adenocarcinoma (PDAC) | MRTX1133, RMC-6236/daraxonrasib, afatinib, SD36 | KRAS, RAF1, EGFR, STAT3 | tumor regression and resistance | targeted therapy

Pancreatic ductal adenocarcinoma (PDAC) has become the third leading cause of cancer-related deaths in the Western World, only second to colorectal and lung cancer (1). These high levels of mortality are mainly attributed to the lack of efficacious therapies. This situation is paradoxical considering the significant progress made during the last two decades on the biology of the disease, mainly thanks to the development of genetically engineered mouse (GEM) tumor models that faithfully reproduce the natural history of the human disease (2, 3). Current therapeutic options available to PDAC patients still rely on cytotoxic drugs such as gemcitabine, approved almost 30 y ago, either alone or in combination with nab-paclitaxel (4). Other highly toxic drug combinations such as FOLFIRINOX offer limited benefit and can only be used in fit patients (5).

KRAS oncogenes, the most common initiating event, were considered undruggable until recently. Efforts to target their canonical signaling pathways such as the mitogen-activated protein kinase (MAPK) and the phosphoinositide 3-kinase (PI3K) cascades have proved to be ineffective in clinical trials due to their high toxicities. This situation took an unexpected turn of events when Shokat and colleagues identified a small pocket in the KRAS protein capable of housing selective inhibitors (6). This discovery led to the development of selective drugs targeting the $KRAS^{G12C}$ isoform, such as sotorasib and adagrasib, which have recently gained FDA approval (7–10). Other noncovalent inhibitors selective for the $KRAS^{G12D}$ isoform have also been generated (11–13). More recently, RAS(ON) inhibitors that block most oncogenic KRAS isoforms as well as their normal counterpart and other members of the RAS family have entered the RAS armamentarium (14–18). One of these inhibitors, the RAS(ON) RMC-6236 inhibitor now known as daraxonrasib, has demonstrated in recent clinical trials to induce a significant increase in patient survival, thus represented a mayor advance for pancreatic cancer patients (18). In experimental tumor models, these RAS(ON) inhibitors, including RMC-6236 and its tool compound RMC-7977, also induced a similar increase in survival, although the mice end up succumbing to the disease due to the appearance of tumor resistance (15–17, 19–20). Hence, in spite of these highly promising results, there is still an urgent need to develop novel and more efficacious therapeutic strategies to induce more robust tumor regressions and to thwart the onset of tumor resistance to prolong the antitumor effect of these novel RAS(ON) inhibitors (21).

Significance

The development of RAS inhibitors represents a major advance in the treatment of KRAS-driven pancreatic ductal adenocarcinoma (PDAC). RAS(ON) inhibitors such as daraxonrasib (RMC-6236) have led to significant improvements in survival compared to historical data. Unfortunately, the rapid onset of tumor resistance has thwarted their therapeutic benefit. This study describes a triple combination therapy made of daraxonrasib along with afatinib, an irreversible EGFR/HER2 kinase inhibitor and SD36, a selective STAT3 PROTAC that induces the robust regression of experimental PDACs and avoids the onset of tumor resistance. This triple combination is well tolerated in mice. Taken together, these studies open the road to design novel combination therapies that may improve the survival of PDAC patients.

[1]V.L. and S.B. contributed equally to this work.

[2]C.G. and M.B. contributed equally to this work.

[3]To whom correspondence may be addressed. Email: mcguerra@cnio.es or mbarbacid@cnio.es.

This article contains supporting information online at https://www.pnas.org/lookup/suppl/doi:10.1073/pnas.2523039122/-/DCSupplemental.

Published December 2, 2025.

Previous studies in our laboratory have illustrated that concomitant ablation of RAF1 and epidermal growth factor receptor (EGFR), two mediators of KRAS signaling, induced complete regression of a limited subset of small mouse GEM PDAC tumors (22). We now report that targeting an additional KRAS signaling node, signal transducer and activator of transcription 3 (STAT3), in combination with RAF1 and EGFR, led to the complete and durable regression of experimental PDAC tumors. More importantly, we have extended these observations to a pharmacological setting by demonstrating that combined inhibition of KRAS, EGFR, and STAT3 induces significant and long-lasting regression of these experimental tumors without inducing significant toxicities.

Results

STAT3 Activation Induces Tumor Resistance upon *Raf1* and *Egfr* Ablation. Previous studies have illustrated that genetic ablation of *Raf*1 and *Egfr* induced the complete regression of a fraction of small PDACs induced in KPeFC mice (*Kras*$^{+/FSFG12V}$;*P53*$^{F/F}$;ElastTA;TetO-Flpo;*Rosa26*CreERT2) (22). We have extended these observations to illustrate that all tumors larger than 100 mm^3 are resistant to *Raf*1 and *Egfr* ablation in vivo (*SI Appendix,* Fig. S1*A*). Interestingly, small and large tumors have similar desmoplastic stroma based on SMA, Vimentin, Collagen, and Masson's Trichrome staining. Likewise, we did not observe significant differences between resistant and sensitive tumors, suggesting that the resistant phenotype is not conveyed by differential stromal composition.

Previous results have illustrated that upon *Raf1* and *Egfr* ablation, STAT3 became activated by phosphorylation on Tyr^{705} (22). To determine whether STAT3 activation had functional consequences for the proliferation of the RAF1/EGFR-resistant tumor cells, we inhibited *Stat3* expression with specific shRNAs before and after elimination of *Raf1* and *Egfr* (Fig. 1*A*). As illustrated in Fig. 1 *A* and *B*, *Stat3* silencing led to the rapid death of the resistant cells, but only in the absence of RAF1 and EGFR expression. Moreover, resistant tumors devoid of RAF1 and EGFR expression displayed increased expression of pSTAT3^{Y705} (Fig. 1*C*). Finally, ectopic expression of STAT3-C/C (STAT3$^{A661C/N663C}$) (23), a constitutively active isoform of STAT3 conferred a resistant phenotype to PDAC cells sensitive to *Raf1* and *Egfr* ablation (Fig. 1 *D* and *E*).

Mechanism of Activation of STAT3. To unveil the mechanism(s) responsible for the activation of STAT3, we first assessed the role of its canonical regulators such as IL6RA and JAK2 (24). Treatment of resistant tumor cells with and without expression of RAF1 and EGFR with four independent JAK1/2 inhibitors (ruxolitinib, itacitinib, tofacitinib, and baricitinib) did not affect cell viability (*SI Appendix,* Fig. S2). Moreover, efficient silencing of *Jak1* and *Jak2* expression either alone or in combination with specific shRNAs had no effect on cell proliferation (Fig. 2*A*). Similar results were obtained when we silenced the IL6 receptor, IL6RA, or *Stat5* (Fig. 2*A*). These results are at variance with those of Miyazaki et al (25) that reports regression of PDAC tumors in xenograft models using the JAK2 inhibitor fedratinib in combination with RAS inhibitors and trametinib, a MEK inhibitor already discarded for human use due to its high toxicity.

Next, we explored the role of the SRC family of kinases in the activation of STAT3 via phosphorylation of residue Tyr^{705}. Immunoprecipitation analysis of lysates of resistant tumor cells expressing or lacking RAF1/EGFR expression with anti-pSRC^{Y419} identified significant levels of phosphorylated SRC proteins in cells lacking RAF1/EGFR expression (Fig. 2*B*). Likewise, we detected increased levels of phosphorylated SRC proteins in tissue sections of KPeFC;*Raf1*$^{\Delta/\Delta}$;*Egfr*$^{\Delta/\Delta}$ tumors compared to those expressing both targets (Fig. 2*C*). Expression analysis of members of this gene family revealed increased expression of *Fyn* (26) in resistant cells (Fig. 2*D*). Indeed, silencing *Fyn* expression with specific shRNAs inhibited the phosphorylation of STAT3 and induced death of resistant tumor cells lacking RAF1 and EGFR expression (Fig. 2*E*).

Combined Ablation of *Raf*1, *Egfr,* and *Stat*3 Induces the Complete and Long-Lasting Regression of Orthotopic Pancreatic Tumors. To interrogate the antitumor effect upon ablation of *Raf1, Egfr,* and *Stat3*, we generated a KPeFC mouse strain carrying conditional alleles for the three targets (22, 27). Tumor cells were obtained from 30 independent tumors. Cells resistant to RAF1/EGFR ablation were identified by dual silencing of RAF1 and EGFR expression with specific shRNAs (*SI Appendix,* Fig. S1 *B* and *C*). Adeno-CRE infection of these resistant KPeFC;*Raf1*$^{L/L}$;*Egfr*$^{L/L}$;*Stat3*$^{L/L}$ tumor cell lines consistently resulted in cell death upon elimination of the three loci. However, elimination of two loci, in all possible combinations, had no effect on tumor cell proliferation (*SI Appendix,* Fig. S1*D*). Hence, expression of just one of the three signaling nodes, either RAF1, EGFR, or STAT3, is sufficient to maintain tumor cell proliferation.

Next, cells derived from nine independent PDACs originally developed in KPeFC mice were orthotopically implanted in immunocompetent C57BL/6 mice (n = 6) since the systemic elimination of STAT3 results in the death of the animals due to intestinal ulcers and peritonitis (*SI Appendix,* Fig. S3) (28–31). The resulting tumor-bearing mice (n = 48) were separated into two cohorts. In one of them (n = 27), we allowed transplanted tumor cells to progress until they reached a volume of 350 to 500 mm^3 (*SI Appendix,* Fig. S4*A*). In the second cohort (n = 21), tumor-bearing mice were exposed to a TMX diet at different tumor sizes (40 to 100 mm^3) to allow CreERT2-mediated recombination of the conditional *Raf1*^{L}, *Egfr*^{L}, and *Stat3*^{L} alleles (Fig. 3 *A* and *B* and *SI Appendix,* Fig. S4*B*). Tumors of TMX-treated mice rapidly underwent apoptotic cell death, as determined by the expression of the active Cleave Caspase 3 (CC3), leading to their complete disappearance in 3 to 4 wk (Fig. 3 *A* and *B* and *SI Appendix,* Fig. S4*B*).

Mice were allowed to thrive without further TMX exposure for up to 300 d postimplantation (Fig. 3*C*). Importantly, none of the 21 PDAC-implanted mice presented detectable tumors during this time. Finally, careful histopathological analysis of their pancreata at the end of the experiment failed to reveal tumoral as well as stromal tissue (Fig. 3*D*). These results illustrate that maintenance of the desmoplastic stroma is completely dependent on the presence of tumor cells. Moreover, they demonstrate that concomitant ablation of three independent targets, *Raf1, Egfr,* and *Stat3,* results in the complete regression of advanced PDACs without the appearance of tumor resistance, one of the main issues thwarting the efficiency of targeted therapies.

Pharmacological Validation of a Combination Therapy of Daraxonrasib, Afatinib, and SD36: In Vitro Studies. Next, we validated this genetic strategy in a pharmacological scenario by using selective inhibitors. First of all, we replaced RAF1 as a target since there are no efficacious RAF1 inhibitors. In contrast, the last few years have witnessed the development of a battery of selective RAS inhibitors, some of which are already yielding promising results in the clinic such as daraxonrasib (RMC-6236) (15–20). This RAS(ON) inhibitor is effective against several KRAS mutant isoforms including KRAS^{G12V}, used in our experimental tumor models (22). As shown in *SI Appendix,* Fig. S5*A*, this RAS inhibitor efficiently blocks ERK phosphorylation but had no effect on either

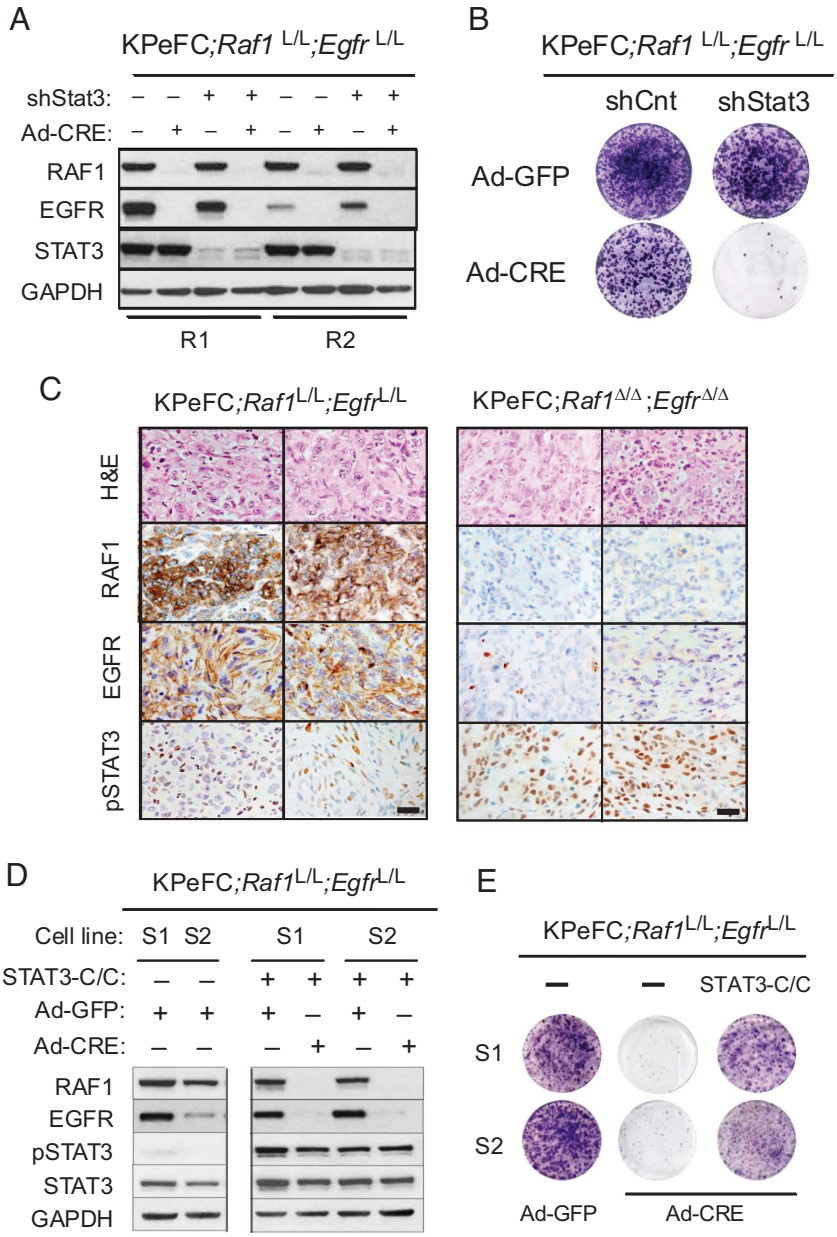

Fig. 1. STAT3 inhibition hinders the proliferation of RAF1/EGFR-resistant tumor cells. (*A*) Western blot analysis of EGFR, RAF1, and STAT3 expression levels in whole cell extracts of two independent RAF1/EGFR-resistant tumor cell lines (R1 and R2) expressing control shRNAs (shStat3−) or shRNAs against STAT3 (shStat3+) followed by infection with Adeno-GFP or Adeno-CRE viral particles. GAPDH served as loading control. (*B*) Colony formation assay of a resistant KPeFC;*Raf1*$^{L/L}$;*Egfr*$^{L/L}$ tumor cell line incubated with control shRNAs or with shRNAs specific for *Stat3* and infected with Adeno-CRE viral particles to eliminate RAF1 and EGFR expression. (*C*) Hematoxylin and eosin (H&E) and IHC analysis of RAF1, EGFR, and pSTAT3^{Y705} expression in tumor sections of representative (*Left*) RAF1/EGFR-resistant KPeFC;*Raf1*$^{L/L}$;*Egfr*$^{L/L}$ tumors (n = 2) or (*Right*) KPeFC;*Raf1* $^{\Delta/\Delta}$;*Egfr*$^{\Delta/\Delta}$ (n = 2) tumors. The scale bar represents 50 μm. (*D*) Western blot analysis of the expression of RAF1, EGFR, pSTAT3, and STAT3 in cell extracts of two independent RAF1/EGFR sensitive KPeFC;*Raf1*$^{L/L}$;*Egfr*$^{L/L}$ tumor cell lines, S1 and S2, ectopically expressing a complementary DNA encoding the constitutively active human STAT3-C/C isoform. Cells were infected with Adeno-GFP or Adeno-CRE viral particles, as indicated. (*E*) Colony formation assay of sensitive KPeFC;*Raf1*$^{L/L}$;*Egfr*$^{L/L}$ S1 and S2 tumor cell lines expressing the human STAT3-C/C isoform and infected with Adeno-GFP or Adeno-CRE viral particles.

the levels of expression of ERK and STAT3 nor activates STAT3 by phosphorylation on Tyr^{705}. To pharmacologically validate EGFR, we first used cetuximab, a monoclonal antibody specific against EGFR (*SI Appendix,* Fig. S5*B*). Unfortunately, this approach failed to mimic the results obtained upon *Egfr* ablation (*SI Appendix,* Fig. S5*C*). Hence, we switched to afatinib, an irreversible tyrosine kinase inhibitor that also blocks the enzymatic activity of the related HER2 receptor (32). Interestingly, the combination of daraxonrasib and afatinib efficiently induced the activation of STAT3 by phosphorylation in Tyr^{705} (*SI Appendix,* Fig. S5 *D–F*), which is responsible for the induction of resistance. These observations indicate that the combined inhibition of KRAS (daraxonrasib) and EGFR (afatinib) has the same consequences as the ablation of R*af1* and E*gfr*. Finally, to pharmacologically validate STAT3, we selected SD36, a specific PROTAC (33).

Subsequent in vitro studies revealed that the combination of daraxonrasib (1 nM), afatinib (0.5 μM), and SD36 (0.5 μM) led to the complete death of PDAC cells in standard colony formation assays. A result reminiscent to that obtained upon ablation of *Raf*1, *Egfr,* and *Stat3* (*SI Appendix,* Fig. S6*A*). Dual-combination treatments only led to partial inhibition of cell proliferation. Among them, those combinations including daraxonrasib displayed the

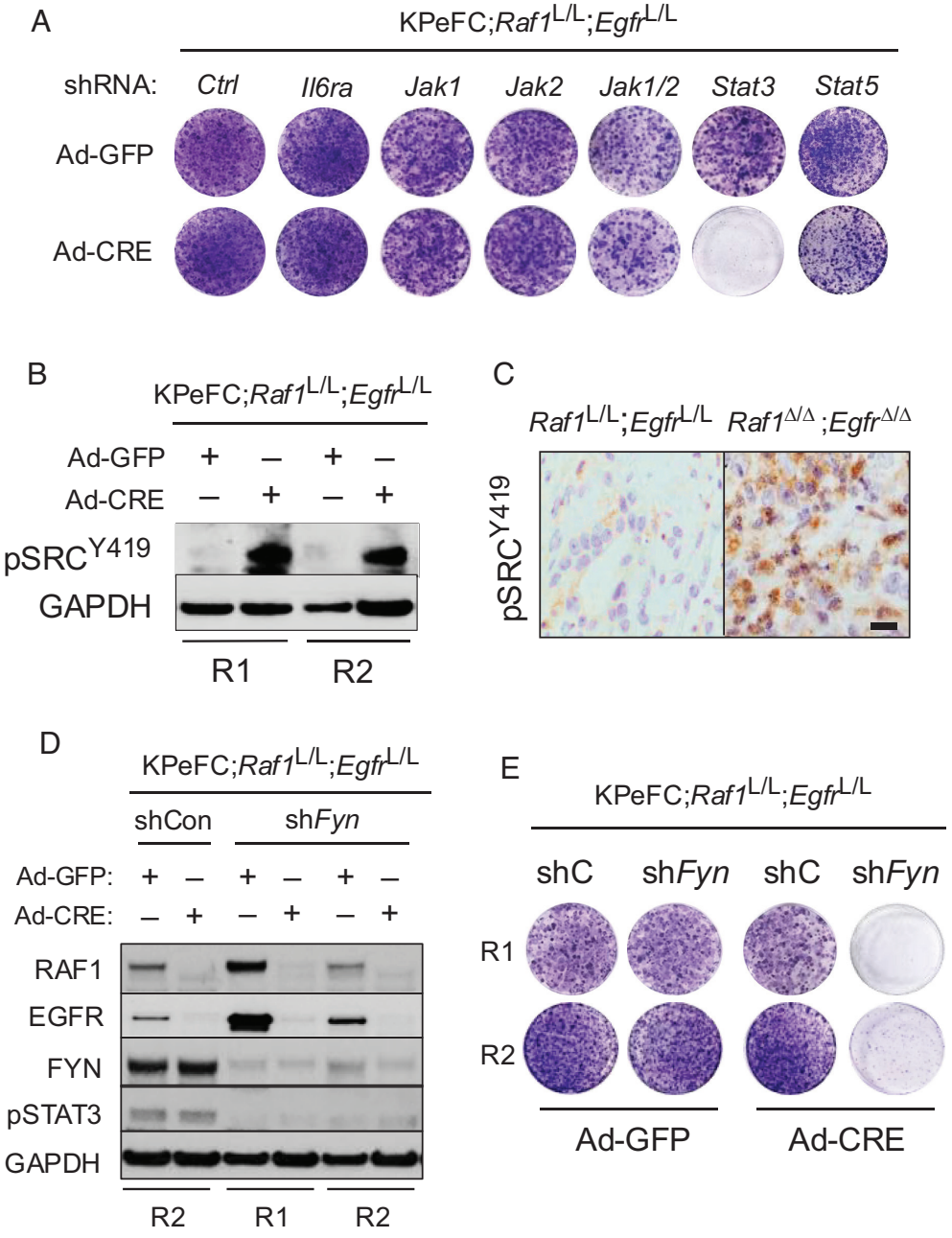

Fig. 2. Mechanism of STAT3 activation in RAF1/EGFR-resistant tumors. (*A*) Colony formation assay of a representative RAF1/EGFR-resistant KPeFC;*Raf1*$^{L/L}$;*Egfr*$^{L/L}$ tumor cell line expressing the indicated shRNAs. Cells were infected with Adeno-GFP or Adeno-CRE viral particles. (*B*) Western blot analysis of phosphorylated members of the SRC family of kinases using a pSRC^{Y419} antibody in whole cell extracts of two independent RAF1/EGFR-resistant (R1 to R2) tumor cell lines infected with Adeno-GFP or Adeno-CRE viral particles. GAPDH was used as loading control. (*C*) IHC analysis of the expression of phosphorylated SRC family members using a pSRC^{Y419} antibody in sections of tumors obtained from representative RAF1/EGFR-resistant KPeFC;*Raf1*$^{L/L}$;*Egfr*$^{L/L}$ and KPeFC;*Raf1* $^{\Delta/\Delta}$;*Egfr* $^{\Delta/\Delta}$ mouse. The scale bar represents 50 μm. (*D*) Western blot analysis of RAF1, EGFR, FYN, and pSTAT3 expression in whole cell extracts of three representative RAF1/EGFR-resistant KPeFC;*Raf1*$^{L/L}$;*Egfr*$^{L/L}$ tumor cell lines (R1 and R2) expressing control shRNAs (shCon) or shRNAs against *Fyn* (sh*Fyn*) after infection with Adeno-GFP or Adeno-CRE viral particles. GAPDH was used as loading control. (*E*) Colony formation assay of the RAF1/EGFR-resistant KPeFC;*Raf1*$^{L/L}$;*Egfr*$^{L/L}$ tumor cell lines shown in *D*, expressing control shRNAs (shC) or shRNAs against *Fyn* (sh*Fyn*). Cells were infected with Adeno-GFP or Adeno-CRE particles as indicated.

highest inhibition levels (*SI Appendix,* Fig. S6*A*). Moreover, the three components of this triple therapy need to be used concomitantly since tumor cell lines made resistant to daraxonrasib failed to respond to the subsequent addition of afatinib and SD36 (*SI Appendix,* Fig. S6*B*). These results suggest that once tumor resistance develops against the KRAS inhibitor, it cannot be reverted by additional exposure to afatinib and SD36.

Pharmacological Validation of the Combination Therapy: In Vivo Studies. To extend these results to an in vivo scenario, cells derived from GEM PDACs were orthotopically implanted in C57BL/6 mice as described above. As expected, untreated tumors grew rapidly, and the mice had to be euthanized at humane endpoint 20 to 40 d postimplantation (Fig. 4*A*). A cohort of implanted mice with PDACs ranging in size from 100 to 200 mm^3 were exposed to daraxonrasib (20 mpk, po, qd) a dose about five times higher than that currently used in clinical trials previously used in similar experimental PDAC tumor models (15, 16) (Fig. 4*A*). Treated tumors displayed effective ERK inhibition and experienced limited growth inhibition that resulted in a significant increase in survival (Fig. 4 *A*, *B*, and *E*). Yet, this cohort of mice ended up succumbing to the disease due to the appearance of tumor resistance. These

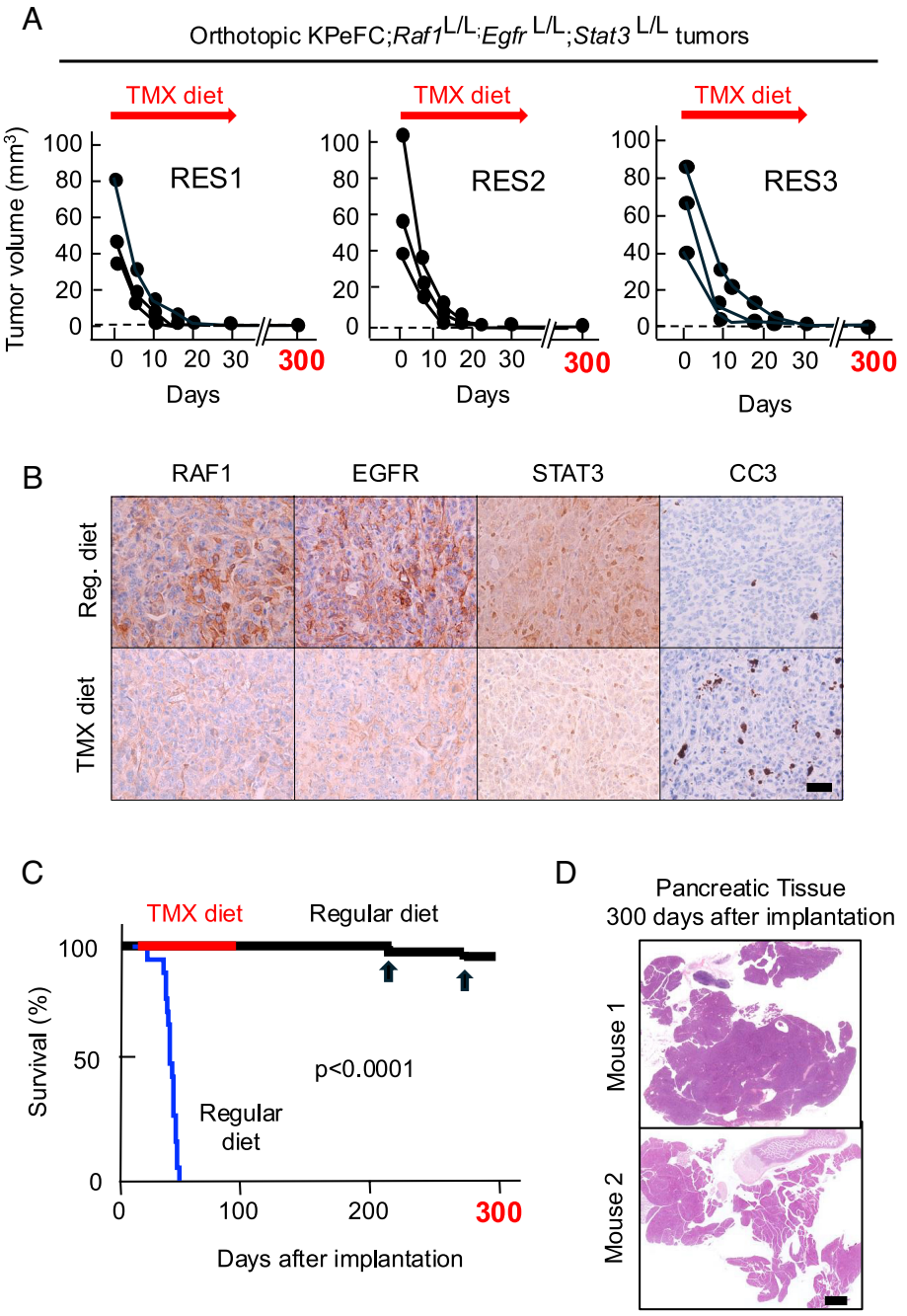

Fig. 3. Complete and durable tumor regressions upon concomitant ablation of *Raf*1, *Egfr*, and *Stat3* in orthotopic pancreatic tumors. (*A*) Tumor volume visualized by ultrasound imaging of tumors present in C57BL/6 mice (n = 3) orthotopically implanted with three RAF1/EGFR-resistant KPeFC;*Raf1*$^{L/L}$;*Egfr*$^{L/L}$;*Stat3*$^{L/L}$ tumor cell lines (RES1 to RES3) exposed to a TMX diet for 30 d (red arrows), when tumors reached 80 to 100 mm^3. Once tumors were no longer detected by ultrasound, mice were fed with regular diet until they reached 300 d postimplantation. The dotted line represents tumor sizes undetectable by ultrasound. (*B*) IHC analysis of RAF1, EGFR, STAT3, and CC3 of tumors of 80 to 100 mm^3 in size after 4 d of exposure to either regular diet or to TMX-containing diet. The scale bar represents 50 μm. (*C*) Kaplan–Meier survival curve of tumor-bearing mice implanted with 12 independent KPeFC;*Raf1*$^{L/L}$;*Egfr*$^{L/L}$;*Stat3*$^{L/L}$ tumor cell lines (three mice per cell line) and either fed with a regular diet (n = 36) (blue line) or exposed to a TMX diet (n = 36) for the indicated time (red line). These mice were fed with a regular diet for 200 additional days (thick solid line). Two mice had to be euthanized at the indicated times (arrows) due to tumor-unrelated causes. The *P* value was obtained using the log-rank Mantel–Cox test, $P < 0.0001$. (*D*) Representative images of H&E-stained sections of pancreatic tissue of two mice exposed to the TMX diet as indicated in *C* and euthanized 300 d postimplantation. No tumoral or stromal tissue could be detected. The scale bar represents 1 mm.

results are reminiscent of those reported by Wasko et al using the tool compound RMC-7977 (15). In contrast, mice treated with the same dose of daraxonrasib along with afatinib (20 mpk, po, qd) and SD36 (50 mpk, ip, qd) underwent rapid apoptotic cell death that resulted in complete tumor regressions (Fig. 4 *C*, *D*, and *F*). Moreover, these mice remained tumor-free for over 200 d posttreatment, indicating that this triple therapy prevented the onset of tumor resistance (Fig. 4 *C*, *E*, and *F*). In contrast, exposure of these tumor-bearing mice to similar treatments made of dual drug combinations including daraxonrasib/afatinib, daraxonrasib/SD36, and afatinib/SD36 did not lead to tumor regressions (*SI Appendix*, Fig. S6*C*). Finally, the combined daraxonrasib/afatinib/SD36 treatment was well tolerated as determined by the lack of weight loss (*SI Appendix*, Fig. S7*A*) and the integrity of the tissues analyzed including the intestinal epithelium, kidney, lung, and spleen (*SI Appendix*, Fig. S7*B*) as well as by the presence of normal blood cell counts (*SI Appendix*, Fig. S7*C*) and metabolic parameters (*SI Appendix*, Fig. S7*D*).

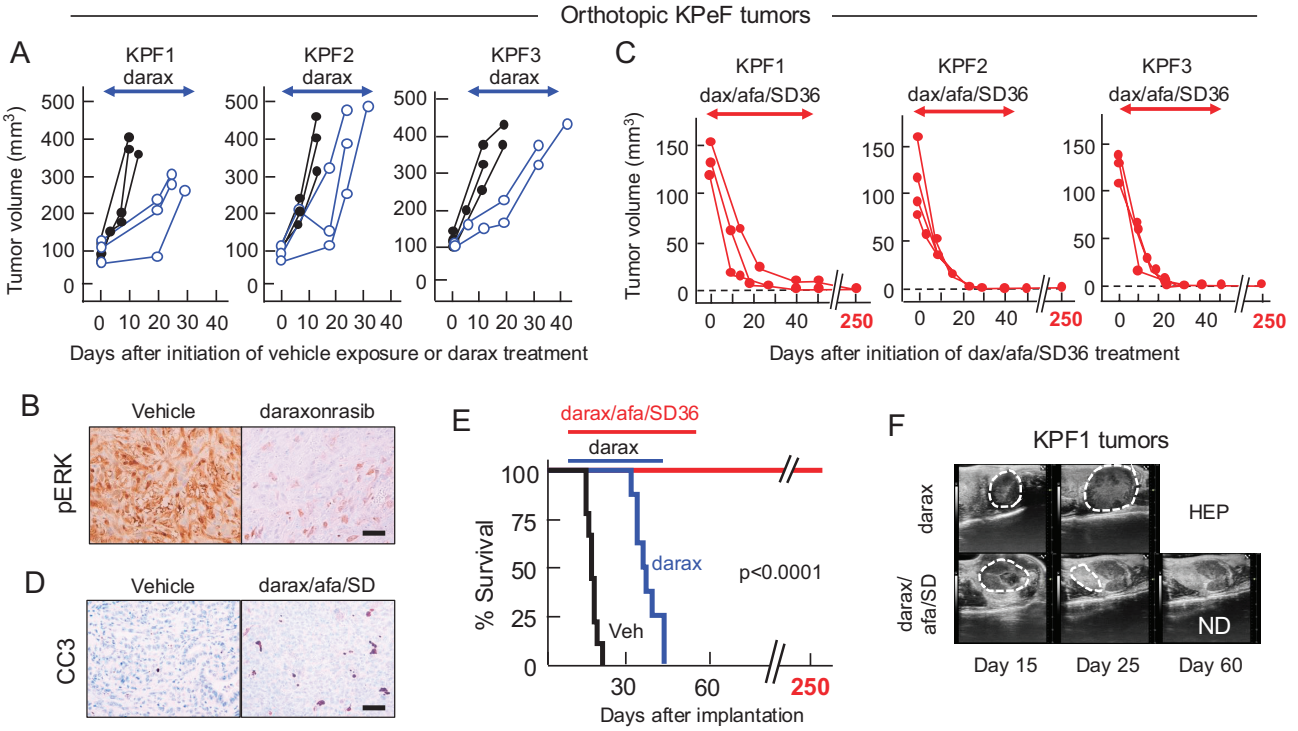

Fig. 4. Combined inhibition of KRAS, EGFR, and STAT3 in orthotopic mouse tumor models also induces complete and durable tumor regressions. (*A*) Tumor volume visualized by ultrasound of orthotopic tumors of C57BL/6 mice implanted with three independent KPeF tumor cell lines (KPF1 to KPF3) treated with vehicle (solid lines) (n = 3) or with the RAS(ON) inhibitor daraxonrasib (20 mpk, po, qd) (blue lines) (n = 3) for the indicated period of time (blue arrowheads). (*B*) Representative IHC analysis of pERK expression in orthotopic KPeF tumors treated with vehicle or daraxonrasib (20 mpk, po, qd) for 4 d. Mice (n = 3) were euthanized 3 h after the treatment. The scale bar represents 50 μm. (*C*) Tumor volume visualized by ultrasound of orthotopic tumors of C57BL/6 mice implanted with three independent KPeF tumor cell lines (KPF1 to KPF3) treated with a combination of daraxonrasib (20 mpk, po, qd), afatinib (20 mpk, po, qd), and SD36 (50 mpk, ip, qd) when the implanted tumors reached 120 to 150 mm^3 in size for up to 50 d (n = 3) (red arrowheads). Mice were allowed to thrive for up to 200 additional days posttreatment. The dotted line represents tumor sizes undetectable by ultrasound. (*D*) IHC analysis of CC3 expression in tumors of around 100 mm^3 (n = 3) exposed for 4 d to vehicle or to the triple combination, daraxonrasib, afatinib, and SD36 and euthanized 3 h after treatment. The scale bar represents 50 μm. (*E*) Kaplan–Meier survival curve of C57BL/6 mice implanted with three independent tumor cell lines (KPF1 to KPF3) treated with vehicle (n = 9) (V, solid line), RAS(ON) inhibitor daraxonrasib (n = 8) (blue line) and a combination of daraxonrasib, afatinib, and SD36 (n = 10) (red line) for the indicated times. Mice were maintained for up to 250 d postimplantation without evidence of tumor resistance. The *P* value was obtained using the log-rank Mantel–Cox test, $P < 0.0001$. (*F*) Representative ultrasound images of the peritoneal cavity of C57BL/6 mice implanted with the KPF-1 tumor cell line and treated with daraxonrasib (darax) or with the combination of daraxonrasib, afatinib, and SD36 (darax/afa/SD) at the indicated times. Tumors are marked with dotted lines. ND, Not Detected. HEP, mouse euthanized at humane endpoint due to large tumor burden.

Alternative Targeted Therapies. The identification of the FYN kinase as a functional activator of STAT3 led us to interrogate the possibility that dasatinib, a well-characterized inhibitor of the SRC family of kinases, may serve as a surrogate for the STAT3 PROTAC, SD36. Dasatinib efficiently inhibited SRC activation as determined by the inhibition of SRC^{Y419} expression both in vitro and in vivo (*SI Appendix,* Fig. S8 *A* and *B*). Indeed, the combination of dasatinib with daraxonrasib and afatinib also induced the robust inhibition of pancreatic tumor cell proliferation in vitro (*SI Appendix,* Fig. S8 *C* and *D*). However, in vivo studies revealed that this triple combination was extremely toxic to the mice. As illustrated in *SI Appendix,* Fig. S8 *E* and *F*, mice treated with these inhibitors displayed gastrointestinal hemorrhages that led to the death of the animals within 24 h posttreatment. Similar toxic results were obtained with related SRC family inhibitors including bosutinib, ponatinib, and tirbanibulin, suggesting that the observed toxicity is mechanism based and not due to off-target effects.

Therapeutic Efficacy of the Combined Daraxonrasib, Afatinib, and SD36 Therapy in GEM Models of PDAC. KPeF mice were monitored until they developed tumors ranging from 100 to 300 mm^3. Mice were randomized into three cohorts and treated with either vehicle, daraxonrasib alone, or with the combination of daraxonrasib, afatinib, and SD36. The results obtained in the vehicle and daraxonrasib monotherapy arms resembled those obtained using orthotopic tumor models in which mice treated with daraxonrasib alone doubled survival but dyed thereafter due to the appearance of tumor resistance (Fig. 5*A*). However, tumor-bearing GEM mice treated with the triple combination of daraxonrasib, afatinib, and SD36 displayed efficient regressions of all tumors enrolled in the study (n = 12), with half of them displaying complete regressions within 30 to 60 d of treatment (Fig. 5 *A* and *B* and *SI Appendix,* Fig. S9 and Table S1). Of importance, none of the 12 mice included in this study experienced tumor relapses at least after 80 to 200 d of treatment (Fig. 5 *A* and *B* and *SI Appendix,* Fig. S9 and Table S1). Whereas GEM tumors reflect more faithfully the human disease, the animals are less fit due to a series of parameters such as increased tumor desmoplasia, unscheduled expression of the KRAS and P53 mutations in other tissues, ectopic expression of the Flpase, systemic K*ras* heterozygosity, and the presence of transgenic alleles, among other characteristics not present in orthotopic tumor models. Thus, a significant fraction of the treated mice had to be euthanized due to tumor-unrelated causes (*SI Appendix,* Table S1). Moreover, since the triple therapy did not cause unfitness in the orthotopic tumor models, it cannot be responsible for the health issues observed in tumor-bearing GEM mice. Finally, as expected, tumor regression was mediated by apoptosis (Fig. 5*C*).

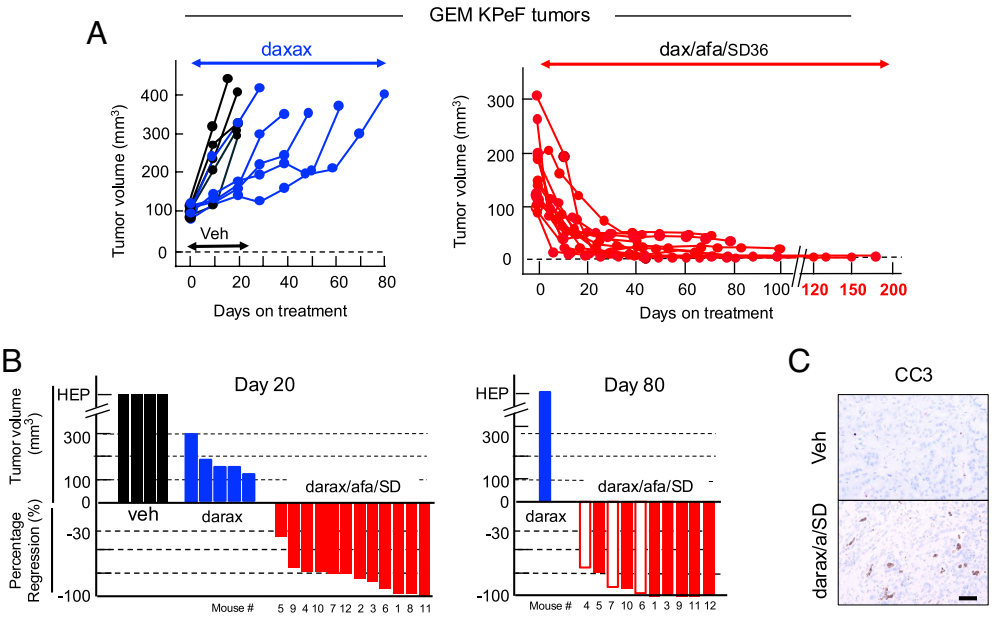

Fig. 5. The triple combination of daraxonrasib, afatinib, and SD36 induces efficient tumor regressions of genetically engineered pancreatic tumors. (*A*) Tumor volume visualized by ultrasound of GEM tumors developed by KPeF mice treated with (*Left*) vehicle (solid lines) (n = 3) or with daraxonrasib (20 mpk, po, qd) (blue lines) (n = 5) and (*Right*) with a combination of daraxonrasib (20 mpk, po, qd), afatinib (20 mpk, po, qd), and SD36 (50 mpk, ip, qd) (red lines) (n = 12). Treatments started when tumors reached at least 100 mm^3 (0 time points). The dotted line represents tumor sizes undetectable by ultrasound. (*B*) Waterfall plot of tumor response of the data shown in A after 20 and 80 d of treatment. (*Left*) Vehicle (solid bars), daraxonrasib (blue bars), the triple combination (red bars). (*Right*) Red empty bars represent the tumor response of the three mice alive after 80 d of treatment. HEP: humane endpoint. (*C*) IHC analysis of CC3 in tumors of around 100 mm^3 in size (n = 4) exposed for 10 d to vehicle or the triple combination, daraxonrasib, afatinib, and SD36 and euthanized 3 h after treatment. The scale bar represents 50 μm.

The Combined Daraxonrasib, Afatinib, and SD36 Therapy Is Active against Patient-Derived Xenograft (PDX) Tumor Models. To study the effect of the triple therapy on tumor cells derived from PDAC patients, we generated seven independent PDX-tumor models from six human PDAC tumors carrying the indicated mutations in *Kras*, *Tp53*, Smad4, and *Cdkn2a* loci (*SI Appendix,* Fig. S10*A*). These PDX tumor models were derived from either human PDAC cells grown in vitro (PDX1-PDX4A) or from tumors directly expanded by subcutaneous implantations of human tumor pieces in immunocompromised mice (PDX4B-PDX6). Fig. 6*A* depicts the additional mutations present in these PDX tumor models based on WES analysis.

In vitro studies using cells derived from PDX1 to three tumors were exposed to daraxonrasib in monotherapy (1 nM) as well as in combination with afatinib (0.5 μM) and SD36 (0.5 μM). As illustrated in *SI Appendix,* Fig. S10*B*, whereas the triple combination completely stopped proliferation of these human tumor cells, daraxonrasib only slowed down tumor progression, a result reminiscent of those obtained with mouse tumor pancreatic cells. A similar study with a different RAS inhibitor, zoldonrasib (RMC-9805) (200 nM), a $KRAS^{G12D}$ investigational drug (34) yielded results similar to those obtained with daraxonrasib (*SI Appendix,* Fig. S10*C*). As previously described in experimental PDACs, we did not observe any therapeutic benefit when we replaced afatinib by cetuximab (*SI Appendix,* Fig. S11*A*). Likewise, a reduction in the dose of afatinib to half also decreased its therapeutic efficacy (*SI Appendix,* Fig. S11*B*). Finally, studies with a different STAT3·PROTAC, KT-333 (35), already under evaluation in clinical trials, gave results similar to SD36 (*SI Appendix,* Fig. S10*D*).

Orthotopic implantation of tumor cells (PDX1-PDX4A tumor models) or subcutaneous implantation of tumor tissue (PDX4B-PDX6 tumor models) in immunocompromised mice led to the rapid appearance of aggressive tumors that forced us to euthanize them at humane endpoint 30 to 40 d after implantation (*SI Appendix,* Fig S12*A*). Histological analysis revealed high levels of cellular heterogeneity and a high percentage of proliferative cells and mitotic figures (*SI Appendix,* Fig. S12 *B* and *C*). Similar results were obtained in tumor-bearing mice treated with vehicle once they reached 80 to 120 mm^3 in size. In contrast, when tumor-bearing mice were exposed to the combination of daraxonrasib (20 mpk, po, qd), afatinib (20 mpk, po, qd), and SD36 (50 mpk, ip, qd), they underwent effective tumor regression in less than 60 d (Fig. 6*B*). No tumor relapses were observed within 80 d posttreatment, suggesting that this triple combination may also prevent the onset of tumor resistance in these human tumor cells.

The presence of the $KRAS^{G12D}$ mutation in the PDX1-3 tumor models allowed us to replace daraxonrasib with the $KRAS^{G12D}$ selective MRTX-1133 inhibitor (11). As illustrated in Fig. 6*C*, the combination of MRTX-1133 (30 mpk, ip, qd) with the same doses of afatinib and SD36 also led to the rapid and complete regression of the PDX tumors. Thus, indicating that the combination therapy described here can work with different KRAS inhibitors. Detailed examination of the pancreas of these treated mice revealed the presence of small cysts (1 to 10 mm^3) lined with low proliferative human ductal-like epithelial cells without atypia in six of the nine mice (Fig. 6*D*). Finally, and as previously shown with mouse tumor models, dual combinations of inhibitors failed to induce tumor repression (*SI Appendix,* Fig. S13). Hence, adding further support to the concept that effective combination therapies such as the one described in this study will require a KRAS inhibitor, afatinib, or a dual EGFR/HER2 inhibitor and a STAT3 degrader. As previously observed with tumors of murine origin, exposure of these human tumor cells to the triple combination also led to the appearance of apoptotic cells. Finally, the combination therapy was well tolerated by the immunocompromised mice as determined by body weight, histological examination of their intestinal epithelium, blood cell counts, and metabolic parameters (*SI Appendix,* Fig. S14). Thus, suggesting that mature immune T cells do not appear to be necessary for the efficient

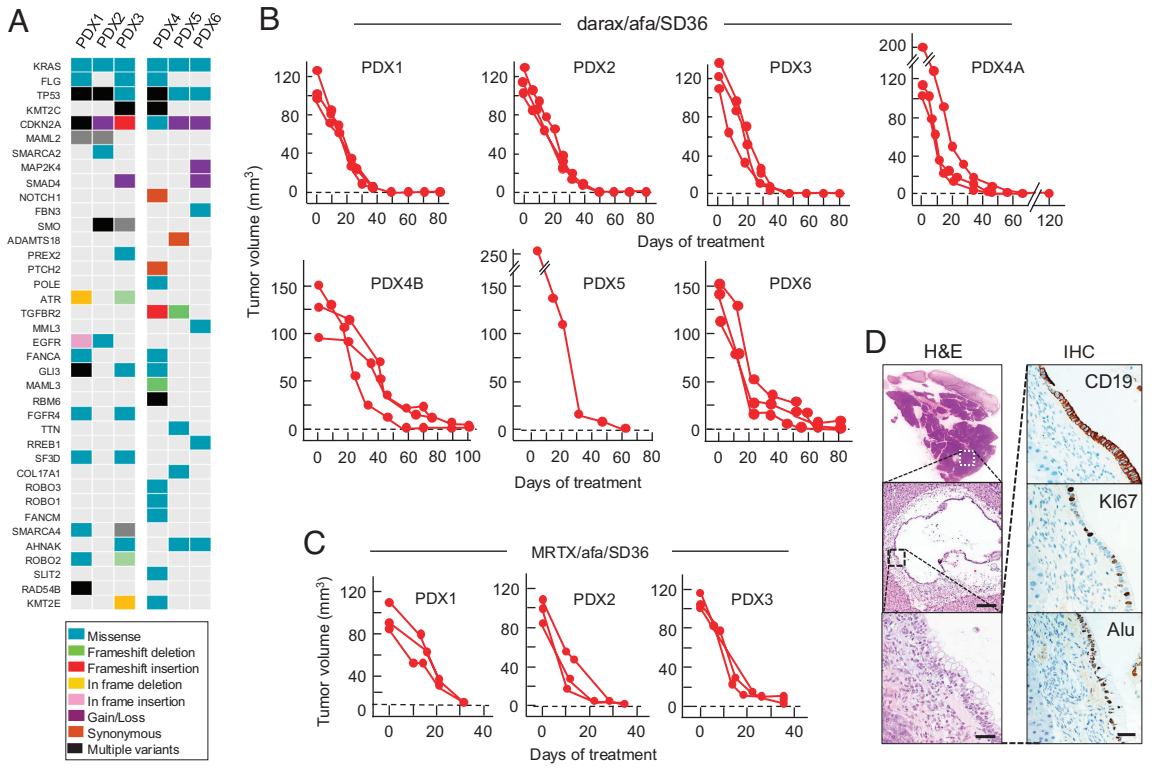

Fig. 6. Therapeutic effect of the combined daraxonrasib, afatinib, and SD36 inhibitors in PDX (*A*, *Top*) Oncoprint indicating the presence of mutated genes in PDXs (PDX1 to PDX6), analyzed by whole exome sequencing (WES). (*Bottom*) The box indicates the color code for the type of mutations. (*B*) Tumor volume of PDX1 to PDX6 tumor models orthotopically implanted in immunodeficient mice (n = 3) and visualized by ultrasound. Mice were treated with a combination of daraxonasib (20 mpk, po, qd), afatinib (20 mpk, po, qd), and SD36 (50 mpk, ip, qd). Treatment was initiated when tumors reached sizes between 100 to 250 mm^3 (0 time points) and maintained until the end of the experiment. (*C*) Tumor volume of PDX1, PDX2, and PDX3 tumor models (n = 3) treated for 30 d with a combination of MRTX-1133 (30 mpk, ip, qd), afatinib (20 mpk, po, qd), and SD36 (50 mpk, ip, qd). Treatment was initiated when tumors reached 100 to 120 mm^3 (0 time points). (*D*, *Top Left*) Representative H&E sections of a pancreas treated with MRTX-1133/afatinib/SD36 as indicated in *C* (the scale bar represents 2 mm). A small cyst is indicated by a dotted square. (*Top Middle*) Magnified section of the cyst shown to the left (the scale bar represents 250 μm). (*Top Right*) Magnified section of the region of the cyst marked with a dotted square (the scale bar represents 50 μm). (*Bottom*) Representative IHC images of CK19, Ki67, and Alu sequences of the cyst shown above. The scale bar represents 50 μm.

induction of tumor regression using the combination therapy described in this study.

Discussion

During the last few years, several RAS inhibitors have been developed including those selective against the $KRAS^{G12C}$ and $KRAS^{G12D}$ isoforms as well as RAS(ON) inhibitors capable of blocking additional isoforms as well as the wild-type RAS proteins (21). The RAS(ON) inhibitors have led to significant tumor regressions and increased survival in mouse tumor models as well as in the clinic (11–20). Regrettably, the therapeutic efficacy of these inhibitors has been thwarted by the rapid appearance of tumor resistance (36). Hence, it will be necessary to develop novel combination therapies that could induce more complete tumor regressions and limit the appearance of tumor relapses (37, 38).

We reasoned that the induction of tumor resistance could be overcome by targeting independent nodes that control KRAS signaling pathways. Indeed, we had already reported the regression of a subset of small GEM PDACs by concomitant ablation of *Raf1* and *Egfr*, two genes encoding downstream and upstream KRAS effectors, respectively (22). As illustrated here, the tumor inhibitory response to *Raf1* and *Egfr* ablation faded away during tumor progression. Moreover, we provide experimental evidence indicating that tumor resistance involves the functional activation of the transcription factor STAT3 via phosphorylation on its regulatory residue, Tyr^{705}. Indeed, resistant tumors lacking RAF1/EGFR expression undergo rapid cell death upon genetic ablation or pharmacological degradation of STAT3. Moreover, ectopic expression of a constitutively active isoform of STAT3 induced resistance to RAF1/EGFR elimination in otherwise sensitive tumor cells.

These observations led us to investigate the therapeutic effect of concomitantly ablating the three signaling nodes, R*af*1, E*gfr*, and S*tat*3. As illustrated here, this strategy led to the rapid regression of mouse pancreatic tumors. Equally important, these animals remained tumor-free for over 200 d indicating that this therapeutic strategy also prevented the onset of tumor resistance over extended periods of time. Interestingly, pancreatic tumor cells maintain their oncogenic properties as long as they retain expression of one of the three signaling nodes. These observations suggest the existence of a complex signaling network that maintains the oncogenicity of pancreatic tumor cells as long as one of these independent nodes remains functionally active.

The absence of selective RAF1 inhibitors initially prevented us from translating those results induced by the concomitant ablation of RAF1, EGFR, and STAT3 expression to a pharmacological scenario. These results led us to replace RAF1 ablation by RAS inhibitors such as daraxonrasib, RAS(ON) inhibitor that has already exhibit promising results in clinical trials. The fact that this inhibitor also affects the wild-type KRAS protein was not considered a problem since recent studies have shown that the systemic K*ras* ablation during adulthood is well tolerated (39). Replacement of EGFR ablation by the anti-EGFR monoclonal antibody cetuximab was unsuccessful. However, afatinib, an irreversible tyrosine kinase inhibitor of EGFR and its related HER2 receptor, was very

effective, suggesting the need to inhibit both receptors. Since afatinib has not been approved for the treatment of PDACs, additional pharmacological strategies need to be tested before attempting to use our triple combination therapy in clinical trials. Indeed, the approved dosing for this inhibitor in PDAC clinical trials of 0.6 mg/Kg is significantly lower than the one used in this study (20 mg/Kg), thus raising questions about the tolerability of this inhibitor in the clinic. On the other hand, the therapeutic efficacy and tolerability of ablating EGFR expression in mice, open the possibility to use EGFR degraders instead of afanitib in the clinic. Finally, STAT3 ablation was successfully replaced by the STAT3 PROTAC SD36. Other PROTACs such as SD91 and KT-333 were equally effective (35). However, STAT3 inhibitors such as C188-9, already in clinical trials, were considerably less effective. The differential effect of STAT3 ablation versus STAT3 degradation is most likely due to the differential consequences of both treatments. Whereas S*tat3* ablation completely eliminates STAT3 expression in an irreversible manner, pharmacological STAT3 degradation is not complete and does not affect the continuous production of the protein, thus maintaining levels of STAT3 expression sufficient to sustain normal homeostasis. Yet, SD36 does not have optimal ADME properties to merit its involvement in clinical trials. Hence, underscoring the need to generate more suitable STAT3 inhibitors specially those orally available.

RAS(ON) inhibitors used as monotherapy have been shown to induce regression of KRAS-driven orthotopic and GEM mouse tumors doubling survival of the treated mice (14–16). More importantly, they are also increasing survival of PDAC patients in phase II clinical trials, thus offering a new and promising alternative to current cytotoxic treatments. Unfortunately, these tumors end up progressing due to the onset of tumor resistance, ultimately leading to the death of the host. We have confirmed these results in orthotopic and GEM tumor models using daraxonrasib in monotherapy. In contrast, our triple combination therapy using daraxonrasib along with EGFR and STAT3 inhibitors not only induced complete and durable tumor regression but efficiently prevented the onset of tumor resistance. Unveiling the mechanism(s) by which this combination of inhibitors prevents tumor resistance may open the door to identify similar strategies for other targeted therapies.

Finally, our triple combination therapy was equally effective in inducing tumor regression in PDX tumor models. Replacement of daraxonrasib by the $KRAS^{G12D}$ selective inhibitor MRTX-1133 also led to complete regressions, indicating that the triple combination maintains its therapeutic activity with different RAS inhibitors. Moreover, these results also shed light on the mechanisms involved in tumor regression. Since PDX tumors are grown in immunodeficient NU-$Foxn1^{nu}$ mice, the observed efficient regression implies that the triple therapy described here exerts its antitumor effects independently of the adaptive immunity provided by the tumor microenvironment.

The road to optimize the triple combination therapy described here to be used in a clinical scenario will not be easy. Yet, it is likely that generation of more efficacious and better tolerated EGFR inhibitors or STAT3 degraders will be available in the near future. Thus, despite current limitations, the results reported here should open the door to new therapeutic options to improve the clinical outcome of PDAC patients in a not-too-distant future.

Methods

Mice. Elas-tTA/TetO-Flpo;*Kras*$^{+/FSFG12V}$;*Trp53*$^{F/F}$;*Raf1*$^{L/L}$;*Egfr*$^{L/L}$;*Rosa26*-CreERT2 mice have been previously described (22). The conditional *Stat3*^{L} allele has also been reported (27). Female and male mice were included in the experiments. Five-week-old female immunodeficient NU-$Foxn1^{nu}$ mice were obtained from Envigo (Indianapolis, IN, USA). All animal experiments were carried out in the animal facility of the CNIO and were approved by the Ethical Committee of the CNIO and the Institute of Health Carlos III. Mice were euthanized according to the International Guidelines for Biomedical Research Involving Animals of the Council for International Organizations of Medical Sciences. All strains were genotyped by TransnetYX (Cordova, TN, USA).

Mouse Pancreatic Tumor Cell Lines. Mouse pancreatic cell lines were generated by freshly resected PDAC tumors minced with razor blades. Tumor pieces were digested in Hank's Balanced Salt Solution (HBSS) (Gibco, USA) supplemented with collagenase P 1.5 μg/mL for 30 min at 37 °C. PDAC cells were cultured in Dulbecco's Modified Eagle Medium (DMEM) (Gibco, USA) supplemented with 10% of fetal bovine serum (Gibco, USA) and 1× Penicillin/Streptomycin (Gibco, USA) and maintained at 37 °C in humidified atmosphere with 5% CO_2. PDAC cells were infected with Adeno-CRE viral particles (multiplicity of infection, 60) and seeded for colony formation assay 5 d after infection. Adeno-GFP particles were used as control. Cells (5,000) were seeded and allowed to form colonies for 10 d. Colonies were fixed with 0.1% glutaraldehyde (Sigma, USA) and stained with 0.5% Crystal Violet (Sigma, USA).

Orthotopic Mouse Tumors. For orthotopic engraftment, 50,000 cells were resuspended in 50 μL of Matrigel (Corning, USA) diluted 1:1 with cold Phosphate-Buffered Saline (PBS) (Gibco, USA). At the beginning of the surgical procedure, the analgesic Buprenorphine and the ophthalmic gel Lacryvisc (Alcon, Switzerland) were applied to mice that were anesthetized with 4% isoflurane (Braun Vetcare, Germany) in 100% oxygen at a rate of 1.5 L/min. Bed heaters were used to avoid hypothermia. After abdominal hair was removed, an incision was made in the left abdominal side, the pancreas was exposed out of the peritoneal cavity, and the cell suspension injected using insulin syringes (30 gauge). The abdominal wall was sutured with absorbable Vicryl suture (Ethicon Inc., USA), and the skin was closed with wound clips (CellPoint Scientific Inc., USA). Tumor volume was assessed weekly by abdominal ultrasound. When tumors reached the appropriate size, mice were randomized and assigned into control/vehicle or treatment groups (n = 3 to 10 per group).

PDX. PDX tumor models were generated from surgically removed human pancreatic tumor samples. We have used three types of PDX tumor models based on the different handling of the human samples including those derived from long-term passaged in culture (22) (PDX1 and PDX2), those grown in culture for 2 to 3 passages for expanding purposes (40) (PDX3 and PDX4A) and those expanded in vivo via subcutaneous implantation (PDX4B, PDX5, and PDX6). For the generation of the PDX1, PDX2, PDX3, and PDX4A tumor models, cell suspensions (100,000 cells) were orthotopically implanted in the pancreas of immunodeficient mice as described above for the corresponding mouse tumors. Tumor volume was assessed weekly by abdominal ultrasound until they reached a volume of at least 100 mm^3 (see below). In the case of the PDX4B, PDX5, and PDX6 tumor models, implanted animals were also monitored until tumors reached similar sizes. Tumor-bearing mice were randomized and assigned into vehicle or treatment groups (n = 3 to 10 per group). Samples are included in registered projects that follow standard operating procedures with the appropriate approval of the Ethics and Scientific Committees (numbers CEIC HCUVA-2013/01, 2011-A01439-32, and CEI 60-1057-A068).

Inhibitors. Daraxonrasib (RMC-6236), MRTX-1133, zoldonrasib (RMC-9805), C188-9, dasatinib, ruxolitinib, itacitinib, tofacitinib, baricitinib, bosutinib, ponatinib, and tirbanibulin were purchased from MedChemExpress (NJ, USA). Afatinib was obtained from Amatek (PA, USA). Cetuximab was purchased from Merck KGaA. SD36 and KT-333 STAT3 PROTACs were synthesized by Vega Oncotargets (Salamanca, Spain). For in vitro experiments, these inhibitors were diluted in dimethyl sulfoxide (DMSO) to final concentration of 10 mM. For in vivo experiments afatinib was dissolved in 0.5% methylcellulose and 0.2% Tween-80 in water, SD36 in 10% polyethylene glycol 400 (PEG400) in PBS and daraxonrasib, MRTX-1133 and dasatinib in 2 to 10% DMSO, 40% PEG300, 5% Tween-80 in saline, according to the guidelines of the manufacturer. Bosutinib, ponatinib, and tirbanibulin were dissolved in 10% DMSO, 40% PEG300, and 5% Tween-80 in saline.

Pharmacological Treatments. Mice carrying conditional alleles were exposed to a tamoxifen-containing diet (TMX) (Tekland TAM^{400}/CreER, Inotiv, USA) to induce their genetic ablation. Mice bearing either orthotopic or GEM tumors were treated with the following inhibitors: daraxonrasib (20 mpk, po, qd), afatinib (20 mpk, po, qd), SD36 (50 mpk, ip, qd), bosutinib (100 mpk, po, qd), ponatinib (30 mpk, po, qd), and

tirbanibulin (25 mpk, po, qd), either alone or in the indicated combinations. PDX models were treated with the following inhibitors: MRTX1133 (30 mpk, ip, qd), daraxonrasib (20 mpk, po, qd), afatinib (10 or 20 mpk, po, qd), SD36 (50 mpk, ip, qd), and cetuximab (0.5 mg, ip, qd), either alone or in the indicated combinations.

Tumor Monitorization. Tumor monitorization was carried out by weekly ultrasounds in the Molecular Imaging Core Unit of CNIO. Mice were anesthetized with 4% isoflurane (Braun Vetcare, Germany) in 100% oxygen at a rate of 1.5 L/min. Bed heaters were used to avoid hypothermia, and abdominal hair was locally removed. Tumors were measured with a High-Resolution system Vevo 770 (Visualsonics, Canada) in an ultrasound transducer of 40 MHz (Visualsonics RMV704, Canada). Tumor sizes were calculated as (Length*Width*Height)/2.

Blood Analysis. Blood was collected from the heart of euthanized mice and transferred to an EDTA-containing tube for hemogram analysis using the Laser Cell blood counter. In parallel, blood also collected from the heart was used for analysis of the metabolic profile with a diagnostic rotor on a VetScan VS2 analyzer.

Immunohistochemistry. Tissue samples were fixed in 10% formalin (Sigma) and embedded in paraffin. For histopathological analysis, specimens were serially sectioned (3 μm thick) and stained with hematoxylin and eosin (H&E). Immunohistochemistry analysis was performed in the Histopathology Unit of CNIO. Antibodies used for mouse tissue include STAT3a (D1A5) (Cell Signaling Technology 8768), EGFR (D1P9C) (Cell Signaling Technology 71655), RAF1 (EM1411E) (Monoclonal Antibodies Core Unit, CNIO), phospho-STAT3 (Y705) (Cell Signaling Technology 9145), phospho-p44/42 MAPK (Cell Signaling Technology 9101), Cleaved Caspase 3 (Cell Signaling Technology 9661), and phospho-SRC (Y419) (Abcam ab4816). For human tissue, the antibodies phospho-STAT3 (Y705) (Cell Signaling Technology 9145), phospho-EGFR (Cell Signaling Technology 2234), Cleaved Caspase 3 (Cell Signaling Technology 9661), Cytokeratin 19 (Agilent IR615), and Ki67 (Agilent IR626) were used. For the antibodies against pSTAT3 and CC3 different dilutions and incubation times were used (1:300, 48 min for mouse tissue and 1:200, 24 min for human tissue). For the detection of Alu sequencies, the nuclear marker Nucleoli (Abcam ab190710) was used. Briefly, for in situ hybridization, sections were deparaffinized and rehydrated. Next, antigen retrieval was performed with the buffer ULTRA CC2 (5424542001, Roche) and discovery protease III (760-2020, Roche). Slides were incubated with the probe AluII (05272041001 Roche) labeled with DNP, followed by stringency washes and incubation with Rabbit anti-DNP (Sigma) conjugated with horseradish peroxidase. Immunohistochemical reaction was developed using DAB+, as a chromogen (ChromoMap DAB, Roche). Finally, nuclei were counterstained with Carazzi's hematoxylin; all the slides were dehydrated, cleared, and mounted with a permanent mounting medium for microscopic evaluation. Stained slides were scanned with the Miraxscanner (Zeiss, Germany), and images were analyzed by the Zen2 software (Zeiss, Germany).

Colony Formation Assays. Infected cells (5,000) were seeded and incubated for 10 d. Colonies were fixed with 0.1% glutaraldehyde (Sigma, USA) and stained with 0.5% Crystal Violet (Sigma, USA). All colony formation assays were performed three times, and all plates were seeded in duplicates.

MTT Viability Assay. Cells were seeded in 96-well plates at a density of 5,000 cells/well. Treatment was started 24 h later for 72 h, and viability rate was determined by the 3-(4,5-dimethylthiazol-2-yl)-2,5-diphenyltetrazolium bromide (MTT) assay (Roche, Switzerland). Absorbance was measured with a microplate reader at 590 nm (EnVision 2104 Multilabel Reader, Perkin Elmer, USA). All samples were measured in triplicates. Graphs represent the average of viability values normalized to the vehicle control. All experiments were performed at least three times.

Western Blot Analysis. Protein extraction was performed on ice with NP-40 lysis buffer supplied with protease and phosphatase inhibitors (cOmplete Mini, Roche; Phosphatase Inhibitor Cocktail 2 and 3, Sigma). To quantify the concentration of protein lysates, the Bradford method (Bio-Rad) was used. 25 μg of cell extracts were loaded and wet transfer was performed using nitrocellulose transfer membrane and transfer buffer (Tris-Glycine 1×, Lonza; MeOH 20%, Panreac), for 70 min at a constant current of 0.40 A. For blocking, membranes were incubated with 5% nonfat milk in TBST [1× Tris-Buffered Saline (TBS) solution, 0.1% Tween-20, Sigma]. Membranes were incubated with primary antibodies diluted in blocking solution overnight at 4 °C. After membranes were washed, they were incubated with HRP secondary antibodies, and protein visualization was done with enhanced chemiluminescent system (ECL Plus, Amersham Biosciences). Membranes were incubated with primary antibodies against EGFR (1:500, Abcam ab52894), RAF1 (1:500, BD Biosciences 610151), STAT3 (1:500, Cell Signaling Technology 9139), phospho-STAT3 (Tyr705) (1:500, Cell Signaling Technology 9131), STAT5 (1:1,000, Cell Signaling Technology 94205), STAT1 (1:1,000, Cell Signaling Technology 9172), phospho-p44/42 MAPK (1:1,000, Cell Signaling Technology 4370), p44/42 MAPK (1:1,000, Cell Signaling Technology 9107), phospho-MEK1/2 (1:250, Cell Signaling Technology 9154), MEK1 (1:1,000, Santa Cruz sc-6250), MEK2 (1:500, BD Biosciences 610235), Cleaved Caspase 3 (1:250, Cell Signaling Technology 9661), Caspase 3 (1:500, Cell Signaling Technology 9662), FYN (1:1,000, Atlas Antibodies HPA023887), phospho-SRC (Y419) (1:500, Abcam ab4816), SRC (1:500, Cell Signaling Technology 2108) and GAPDH (1:5,000, Sigma G8795), VINCULIN (1:1,000, Sigma-Aldrich V9131), and ACTIN (1:1,000, Sigma-Aldrich A5441) as loading controls. Anti-mouse HRP-linked (1:2,000, Agilent Dako P0447) and anti-rabbit HRP-linked (1:2,000, Agilent Dako P0448) were used as secondary antibodies. For the quantification of protein expression, the intensity of the bands was quantified with ImageJ2.

Data, Materials, and Software Availability. All study data are included in the article and/or *SI Appendix*. No code or sequencing data were generated. For data, material or further information contact mcguerra@cnio.es.

ACKNOWLEDGMENTS. We thank R. Villar for excellent technical assistance and I. Aragón, V. Viñas, and I. Blanco (Animal Facility), F. Mulero, G. Visdomine, and G. Medrano (Molecular Imaging Unit), P. Gonzalez (Histopathology Unit), and O. Dominguez (Genomic Unit) of CNIO for their excellent technical support. We also thank J. de la P. and E. Ortiz from the Servicio de Anatomía Patológica of the *Hospital Clínico Universitario Virgen de la Arrixaca* (HCUVA) (Murcia) and the Biobank of the *Instituto Murciano de Investigación Biosanitaria* (IMIB) (PT23/00026; Platform ISCIII Biomodels and Biobanks) for providing clinical samples. This work was supported by grants from the CRIS Cancer Foundation, the European Research Council (ERC-AG/695566-THERACAN), the *Agencia Estatal de Investigación* cofunded with the European Regional Development Fund (ERDF-EU ERDF) (PID2021-124106OB-I00; MCIU/AEI/10.13039/501100011033), and the European Union "NextGenerationEU"/PRTR" (PLEC2022-009255;MCIU/AEI/10.13039/501100011033) to M.B. C.G. and M.B. are recipients of a CIBERONC Fund (CB21/12/00121). Additional funding included grants from the *Instituto de Salud Carlos III* cofunded by ERDF (PI19/00514), the "*Carmen Delgado/Miguel Pérez Mateo Grants* of the *"Asociación Cancer de Páncreas*" to C.G., the Italian Cancer Research Association (AIRC, IG16930), and the Italian Ministry of University and Research (MIUR PRIN 2017) to V.P. M.B. is the recipient of an Endowed Chair from the AXA Research Fund. V.L. was supported by an INPhINIT fellowship from "La Caixa" Foundation (LCF/BQ/DI18/11660011) and a contract from the CRIS Cancer Foundation. S.B. is supported by a PhD scholarship from the Foundation of Science and Technology of Portugal (10.54499/2021.05875.BD). M.K. was supported by an Erasmus+ scholarship for traineeship. L.M.-C. was supported by an FPU fellowship from the *Ministerio de Educación*. J.C.L-G. is supported by a postdoctoral fellowship from *Amigos del CNIO*, E.Z.-D. is supported by a FPI fellowship (PRE2022-102952) from the Spanish Ministry of Sciences and Innovation (PID2021-124106OB-I00). P.S. is partially supported by a fellowship from the China Scholarship Council.

Author affiliations: [a]Experimental Oncology Group, Tumor Biology Program, Centro Nacional de Investigaciones Oncológicas, Madrid 28029, Spain; [b]Centro de Investigación Biomédica en Red Cancer (CIBERONC), Madrid 28029, Spain; [c]Molecular Mechanisms of Cancer Program, Centro de Investigación del Cáncer and Instituto de Biología Molecular y Celular del Cáncer, Consejo Superior de Investigaciones Científicas-Universidad de Salamanca (CSIC-USAL), Salamanca 37007, Spain; [d]Cancer Stem Cells and Fibroinflammatory Microenvironment Group, Instituto de Investigaciones Biomédicas Sols-Morreale Consejo Superior de Investigaciones Científicas-Universidad Autónoma de Madrid (CSIC-UAM), Madrid 28029, Spain; [e]Biomarkers and Personalized Approach to Cancer Group, Area 3 Cáncer, Instituto Ramón y Cajal de Investigación Sanitaria, Madrid 28049, Spain; [f]Department of Biochemistry and Molecular Biology, Faculty of Pharmacy, Universidad Complutense, Madrid 28040, Spain; [g]Cancer and Obesity Group, Instituto de Investigación Sanitaria Hospital Clínico San Carlos, Madrid 28040, Spain; [h]Histopathology Unit, Biotechnology Program, Centro Nacional de Investigaciones Oncológicas, Madrid 28029, Spain; [i]Centre de Recherche en Cancérologie de Marseille, INSERM U1068, CNRS UMR 7258, Aix-Marseille Université and Institut Paoli-Calmettes; Parc Scientifique et Technologique de Luminy, Marseille 13288, France; [j]Molecular Biotechnology Center and Department of Molecular Biotechnology and Health Sciences, University of Turin, Turin 101214, Italy; and [k]Department of Surgery, Hospital Clinico Universitario Virgen de la Arrixaca and Instituto Murciano de Investigación Biomédica, Murcia 30120, Spain

Author contributions: V.L., C.G., and M.B. designed research; V.L., S.B., M.K., C.G.L., E.Z.-D., D.A., L.M.-C., P.S., B.R.-P., R.B., S.J.-P., A.L.-G., M.S.R., and J.C.L.-G. performed research; B.S., N.D., V.P., and F.S.-B. contributed new reagents/analytic tools; V.L., S.B., R.A., M.D., M.M., E.C., and C.G. analyzed data; M.D. and M.M. provided critical input; and V.L., S.B., C.G., and M.B. wrote the paper.

Reviewers: A.B., Netherlands Cancer Institute; I.G.-L., Professor of Oncology at the University of Utah School of Medicine and Director of the Phase I Program at Huntsman Cancer Institute; and D.A.T., Cold Spring Harbor Laboratory Cancer Center.

Competing interest statement: V.L. and C.G. declare an International Patent Application PCT/EP2024/052345 and a European Patent Application No. 23382078.6 entitled "Triple combined therapy inhibiting EGFR, RAF1 and STAT3 against pancreatic ductal adenocarcinoma." V.L., C.G., and M.B. declare a European Patent Application No. 25382815.6. entitled "Novel Therapy." Reviewer I.G.-L. notes the following: "I am a principal investigator in the first-in-human trial with RMC-6236 (Daraxonrasib) as well as PI in the randomized phase 3 trial (RASOLUTE-302) comparing RMC-6236 to standard chemotherapy in patients with metastatic pancreatic cancer in the second line. I have received consulting fees for participating in advisory boards for Revolution Medicine.".

1. R. L. Siegel, K. D. Miller, N. S. Wagle, A. Jemal, Cancer statistics, 2023. *CA Cancer J. Clin.* **73**, 17–48 (2023).
2. P. A. Pérez-Mancera, C. Guerra, M. Barbacid, D. A. Tuveson, What we have learned about pancreatic cancer from mouse models. *Gastroenterology* **142**, 1079–1092 (2012).
3. M. Drosten, C. Guerra, M. Barbacid, Genetically engineered mouse models of K-Ras-driven lung and pancreatic tumors: Validation of therapeutic targets. *Cold Spring Harb. Perspect. Med.* **8**, a031542 (2018).
4. D. D. Von Hoff *et al.*, Increased survival in pancreatic cancer with nab-paclitaxel plus gemcitabine. *N. Engl. J. Med.* **369**, 1691–1703 (2013).
5. T. Conroy *et al.*, FOLFIRINOX or gemcitabine as adjuvant therapy for pancreatic cancer. *N. Engl. J. Med.* **379**, 2395–2406 (2018).
6. J. M. Ostrem *et al.*, K-Ras(G12C) inhibitors allosterically control GTP affinity and effector interactions. *Nature* **503**, 548–551 (2013).
7. F. Skoulidis *et al.*, Sotorasib for lung cancers with *KRAS* p. G12C mutation. *N. Engl. J. Med.* **384**, 2371–2381 (2021).
8. P. A. Jänne *et al.*, Adagrasib in Non-Small-Cell Lung Cancer Harboring a *KRASG12C* Mutation. *N. Engl. J. Med.* **387**, 120–131 (2022).
9. R. Yaeger *et al.*, Adagrasib with or without cetuximab in colorectal cancer with mutated *KRAS* G12C. *N. Engl. J. Med.* **388**, 44–54 (2023).
10. J. H. Strickler *et al.*, Sotorasib in *KRAS* p. G12C-mutated advanced pancreatic cancer. *N. Engl. J. Med.* **388**, 33–43 (2023).
11. J. Hallin *et al.*, Anti-tumor efficacy of a potent and selective non-covalent $KRAS^{G12D}$ inhibitor. *Nat. Med.* **28**, 2171–2182 (2022).
12. K. C. M. Gulay *et al.*, Dual inhibition of KRASG12D and pan-ERBB is synergistic in pancreatic ductal adenocarcinoma. *Cancer Res.* **83**, 3001–3012 (2023).
13. S. B. Kemp *et al.*, Efficacy of a small-molecule inhibitor of KrasG12D in immunocompetent models of pancreatic cancer. *Cancer Discov.* **13**, 298–311 (2023).
14. D. Kim *et al.*, Pan-KRAS inhibitor disables oncogenic signalling and tumour growth. *Nature* **619**, 160–166 (2023).
15. U. N. Wasko *et al.*, Tumour-selective activity of RAS-GTP inhibition in pancreatic cancer. *Nature* **629**, 927–936 (2024).
16. M. Holderfield *et al.*, Concurrent inhibition of oncogenic and wild-type RAS-GTP for cancer therapy. *Nature* **629**, 919–926 (2024).
17. J. Jiang *et al.*, Translational and therapeutic evaluation of RAS-GTP inhibition by RMC-6236 in RAS-driven cancers. *Cancer Discov.* **14**, 994–1017 (2024).
18. K. C. Arbour *et al.*, 652o preliminary clinical activity of RMC-6236, a first-in-class, RAS-selective, tri-complex RAS-MULTI(ON) inhibitor in patients with *KRAS* mutant pancreatic ductal adenocarcinoma (PDAC) and non-small cell lung cancer (NSCLC). *Ann. Oncol.* **34**, S458 (2023).
19. M. I. Orlen *et al.*, T-cell dependency of tumor regressions and complete responses with RAS(ON) multi-selective inhibition in preclinical models of PDAC. *Cancer Discov.* **15**, 1697–1716 (2025).
20. C. Broderick *et al.*, A RAS(ON) multi-selective inhibitor combination therapy triggers long-term tumor control through senescence-associated tumor-immune equilibrium in pancreatic ductal adenocarcinoma. *Cancer Discov.* **15**, 1717–1739 (2025).
21. K. Drizyte-Miller *et al.*, KRAS: The Achilles' heel of pancreas cancer biology. *J. Clin. Invest.* **135**, e191939 (2025).
22. T. M. Blasco *et al.*, Complete regression of advanced pancreatic ductal adenocarcinomas upon combined inhibition of EGFR and C-RAF. *Cancer Cell* **35**, 573–587 (2019).
23. J. F. Bromberg *et al.*, Stat3 as an oncogene. *Cell* **98**, 295–303 (1999).
24. D. E. Johnson, R. A. O'Keefe, J. R. Grandis, Targeting the IL-6/JAK/STAT3 signalling axis in cancer. *Nat. Rev. Clin. Oncol.* **15**, 234–248 (2018).
25. S. Miyazaki *et al.*, Targeting *KRAS*-mutant pancreatic cancer through simultaneous inhibition of *KRAS*, *MEK*, and *JAK2*. *Mol. Oncol.* **19**, 377–390 (2025).
26. M. D. Resh, Fyn, a Src family tyrosine kinase. *Int. J. Biochem. Cell Biol.* **30**, 1159–1162 (1998).
27. T. Alonzi *et al.*, Essential role of STAT3 in the control of the acute-phase response as revealed by inducible gene inactivation [correction of activation] in the liver. *Mol. Cell. Biol.* **21**, 1621–1632 (2001).
28. T. Alonzi *et al.*, Induced somatic inactivation of STAT3 in mice triggers the development of a fulminant form of enterocolitis. *Cytokine* **26**, 45–56 (2004).
29. G. Pickert *et al.*, STAT3 links IL-22 signaling in intestinal epithelial cells to mucosal wound healing. *J. Exp. Med.* **206**, 1465–1472 (2009).
30. J. R. Matthews, O. J. Sansom, A. R. Clarke, Absolute requirement for STAT3 function in small-intestine crypt stem cell survival. *Cell Death Differ.* **18**, 1934–1943 (2011).
31. L. Pang *et al.*, STAT3 signalling via the IL-6ST/gp130 cytokine receptor promotes epithelial integrity and intestinal barrier function during DSS-induced colitis. *Biomedicines* **9**, 187 (2021).
32. N. Minkovsky, A. Berezov, BIBW-2992, a dual receptor tyrosine kinase inhibitor for the treatment of solid tumors. *Curr. Opin. Investig. Drugs* **9**, 1336–1346 (2008).
33. L. Bai *et al.*, A potent and selective small-molecule degrader of STAT3 achieves complete tumor regression in vivo. *Cancer Cell* **36**, 498–511 (2019).
34. C. Weller *et al.*, A neomorphic protein interface catalyzes covalent inhibition of RAS^{G12D} aspartic acid in tumors. *Science* **389**, eads0239 (2025).
35. P. Liu *et al.*, A fiist-in-class STAT3 degrader KT-333 in development for treatment of hematologic cancers. *Blood* **138**, 1865 (2021).
36. J. Dilly *et al.*, Mechanisms of resistance to oncogenic *KRAS* inhibition in pancreatic cancer. *Cancer Discov.* **14**, 2135–2161 (2024).
37. A. J. Aguirre *et al.*, Hope on the horizon: A revolution in KRAS inhibition is creating a new treatment paradigm for patients with pancreatic cancer. *Cancer Res.* **84**, 2950–2953 (2024).
38. A. Mullard, Wrestling with the RAS cancer drug pipeline. *Nat. Rev. Drug Discov.* **24**, 242–243 (2025).
39. E. Zamorano-Dominguez *et al.*, Systemic Kras ablation disrupts myeloid cell homeostasis in adult mice. *Proc. Natl. Acad. Sci. U.S.A.* **122**, e2512404122 (2025).
40. R. Nicolle *et al.*, Pancreatic adenocarcinoma therapeutic targets revealed by tumor-stroma cross-talk analyses in patient-derived xenografts. *Cell Rep.* **21**, 2458–2470 (2017).